HHS Public Access

Author manuscript

Microporous Mesoporous Mater. Author manuscript; available in PMC 2019 October 01.

Published in final edited form as:

Microporous Mesoporous Mater. 2018 October ; 269: 156–159. doi:10.1016/j.micromeso.2017.05.030.

Using double pulsed-field gradient MRI to study tissue microstructure in traumatic brain injury (TBI)

Michal E Komlosh[a,b,*], **Dan Benjamini**[a], **Elizabeth B Hutchinson**[a,b], **Sarah King**[a,b], **Margalit Haber**[c], **Alexandru V Avram**[a], **Lynne A Holtzclaw**[e], **Abhishek Desai**[d], **Carlo Pierpaoli**[a], and **Peter J Basser**[a]

[a]Section on Quantitative Imaging and Tissue Sciences, NICHD, National Institutes of Health, Bethesda, MD, USA

[b]Center for Neuroscience and Regenerative Medicine, Uniform Service University of the Health Sciences, Bethesda, MD, USA

[c]Department of Neurology, University of Pennsylvania, Philadelphia, PA, USA

[d]Laboratory of Molecular Signaling, NIAAA, National Institutes of Health, Rockville, MD, USA

[e]Microscopy and Imaging Core, NICHD, National Institutes of Health, Bethesda, MD, USA

Abstract

Double pulsed-field gradient (dPFG) MRI is proposed as a new sensitive tool to detect and characterize tissue microstructure following diffuse axonal injury. In this study dPFG MRI was used to estimate apparent mean axon diameter in a diffuse axonal injury animal model and in healthy fixed mouse brain. Histological analysis was used to verify the presence of the injury detected by MRI.

Graphical abstract

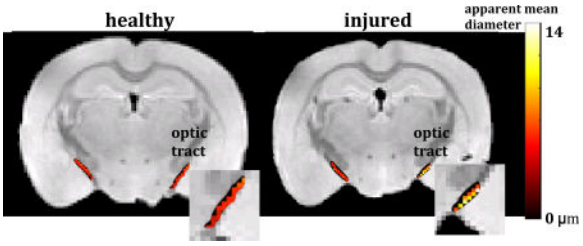

Keywords

anisotropic diffusion; MRI; microstructure; diffusion; d-PFG; DDE; DTI; TBI; DAI; CHIMERA

[*]Corresponding author. Phone: +1-301-435-3868, komloshm@mail.nih.gov (Michal E Komlosh).

1. Introduction

Traumatic brain injury (TBI) is a major cause of disability and death worldwide, accounting for about 30% of all injuries related deaths in the USA [1]. One of the most common pathologies which is present in about 40%–50% of cases of traumatic brain injury (TBI) cases is diffuse axonal injury (DAI) [2], resulting in preferential damage to white matter [3]. DAI ranges from mild to severe, and is accompanied by tissue microstructural alterations including axonal abnormalities such as varicosities and axonal loss, as well as gliosis and microglia cell infiltration [4, 5]. While clinical MRI is routinely used to detect gross anatomical and vascular abnormalities, the subtle white matter changes associated with DAI are challenging to diagnose and characterize using conventional MRI methods. Often DAI can only be detected at autopsy [2]. Diffusion MRI methods such as diffusion tensor imaging (DTI) [6] show promise for probing subtle changes in brain microstructure [7–9], however, the resulting metrics such as fractional anisotropy (FA), and mean diffusivity (MD) lack sufficient specificity to suggest the biophysical origin of these changes. Diffusion correlation methods such as double pulsed-field gradient (dPFG) [10, 11], illustrated in Figure 1, in which the MRI signal is sensitized to displacement correlations rather than the mean-squared net displacements, may improve both sensitivity and specificity in detecting brain abnormalities following injury. In the central nervous system (CNS), dPFG data may be used to characterize features of a cylindrical pack of axons that constitute white matter fascicles. By using a dPFG variant with vanishing mixing time between the two diffusion encoding blocks (i.e., $\tau_m = 0$) average axon diameter (AAD) [12–15] or axon mean diameter (AMD) and axon diameter distribution [16, 17] can be estimated.

The objective of this study was to apply a 3D implementation of the dPFG acquisition and modeling of axon diameters to a recently developed closed-head impact model of engineered rotation acceleration (CHIMERA) that induces DAI in the mouse brain in select white matter tracts, including the optic tract [5]. We present pilot results in using the dPFG method to detect cellular alterations in the CHIMERA injury model by comparison of the more conventional FA metric computed from DTI with the AMD metric in the optic tract.

2. Materials and Methods

All animals were housed and treated according the national animal care guidelines and institutional oversight by the NIH/NIAAA IACUC. Brain specimens were obtained from two mice (C57BL/6N, males), one following CHIMERA injury and one with a sham injury (i.e., placed in device, but without impact). The CHIMERA [5] involves delivering an impact of a defined energy to a mouse head. During impact head motion is not constrained. The injury is caused by shear force developing within the brain following impact. Note, this injury model affects predominantly white matter while the skull remains intact. The injury was induced with 0.5J impact energy and repeated three times with 24 hour interval between injuries. One week after the third injury, mice underwent transcardial perfusion with cold 4% formaldehyde in PBS and the fixed brains were removed from the skull. Following a 24 hour post-fixation period in 4°C, brains were rehydrated and stored in PBS with % sodium azide prior to MRI scanning.

All experiments were performed on a 7 T Bruker vertical wide-bore magnet with an AVANCE III MRI spectrometer equipped with a Micro2.5 microimaging probe and three GREAT60 gradient amplifiers, which have a nominal peak current of 60 A per channel. This configuration can produce a maximum nominal gradient strength of 24.65 mT m^{-1} A^{-1} along each of the three orthogonal directions. The ambient temperature of the magnet bore was 16.8°C.

Diffusion tensor imaging (DTI) MRI data were acquired using a 3D EPI MRI sequence with the following MRI parameters: echo time (TE)/ repetition time (TR)=23/700 ms, 8 segments, and voxel resolution of 100 100 100 μ_m^3; DTI parameters were: gradient pulse duration, δ, of 3 ms, diffusion time, Δ, of 20 ms, and the b-value ($b = \gamma^2\delta^2G^2[\Delta\ \delta/3]$, where γ is the gyromagnetic ratio and G is the diffusion gradient amplitude) of 400 and 2000 s mm^{-1}. DPFG imaging parameters were acquired with the same imaging parameters as the DTI. The dPFG filter parameters were $\tau_m = 0$, δ 3 ms, and Δ = 20 ms. To define the diffusion gradient orientations in space, a spherical coordinate system was used. The angle between the two pulsed-field gradient (PFG) blocks, φ, was applied twice −0° and 180° for each orientation [14]. The diffusion data were acquired on three shells, representing different diffusion amplitudes, with q values ($q = \gamma G\delta/2\pi$) of 84.8, 71.6, and 56.6 mm^{-1}, each with 37, 16, and 7 uniformly distributed orientations on a hemisphere, respectively. The directions along each shell are independent of the other shells, providing additional spatial and directional information due to more homogeneous sampling of the space. A comprehensive description, including the pulse sequence scheme and gradient orientations, is provided elsewhere [14].

High resolution T2-weighted images were acquired to serve as anatomical templates for registration of the DTI and dPFG data during correction for image distortions/artifacts due to the EPI acquisition. A 3D spin echo sequence was used with TE/TR = 40/2000 ms, voxel resolution of 100 100 100 μm^3. First, the Diffusion-weighted data were registered to the T_2-weighted structural image and processed using the TORTOISE software package [19]. Non-linear fitting was used to calculate the DTI metrics such as the eigenvectors, FA maps, mean and axial diffusivities, and the amplitude image with no diffusion sensitization ($A_{b=0}$). Manual segmentation was performed on $A_{b=0}$ of the injured and sham brains to define the optic tract region of interest (ROI), resulting in left and right optic tracts ROIs (total of four) later to be used to calculate the mean FA and AMD. To perform a voxelwise estimation of the AMD, the optic tract axons were modelled as a pack of impermeable parallel cylinders of infinite length with a known orientation. The dPFG signal attenuation from the restricted compartment (i.e., axons) was computed using the multiple correlation function (MCF) method [20–22]. In addition to diffusion within the axons, the extra-axonal diffusion was modeled as Gaussian [23]. DTI-derived metrics were used to reduce the complexity of the AMD estimation model. In each voxel, the tensor's main eigenvector was assumed to indicate the orientation of the par-allel cylinders [14]. In addition, the DTI-derived mean and axial diffusivities were assumed to be the intra-and extra-axonal diffusivities in the AMD estimation, respectively. All data processing was performed with in-house code written in MATLAB (The Mathworks, Natick, MA).

Immunohistochemistry for axonal neurofilament protein was performed in slices from each brain containing the optic tract to detect the presence of axonal varicosities in this location. After a cryoprotection by a series of sucrose solutions, brains were frozen and cryosectioned with 20 μm slice thickness. Floating sections in which the optic tract was evident were selected for IHC using the primary antibody rabbit anti-NF light chain (Cell Signaling #2837, Danvers, MA, 1:200) and secondary an-tibody Alexa Fluor 488 (Thermo Fisher, Waltham, MA, 1:500). Stained sections were imaged using a Zeiss 700 laser scanning confocal microscope with FITC filters and a 63x** oil immersion objective. Images were acquired for the left and right optic tract of each brain.

3. Results and Discussion

Figure 2 shows the DTI fractional anisotropic (FA) (a–b) and dPFG AMD (c–d) maps of the optic tract overlay a structural image of the sham (a, c) and CHIMERA (b, d) mouse brains. ROIs comprising the optic tract show mean FA of 0.66 and 0.75 for the right and left optic tract of the CHIMERA, and 0.79 and 0.78 for the right and left optic tract of the sham, respectively. The lower FA value of the right CHIMERA optic tract vs. the sham is consistent with injury at this location [24]. ROI analysis of the dPFG data shows AMD of 8.6 μm and 5.4 μm for the right and left optic tracts of the CHIMERA and 4.8 μm and 5.2 μm of the right and left optic tract of the sham, respectively. The estimated AMD of the right CHIMERA brain is noticeably larger compared with than that of the sham mouse. Figure 3 shows a histogram of the AMDs within the optic tracts. Note the tight distribution of diameters in the sham and left optic tract of the CHIMERA while the right optic tract shows a broader distribution of diameters. Both the AMD map and the histogram of the right CHIMERA brain points to an axonal damage at the same site detected by DTI, indicating alteration in the tissue microstructure are likely due to axonal varicosities and axonal loss. The left optic tract of the CHIMERA shows no significant decrease of FA, nor increase of AMD, suggesting an asymmetrical degree of severity of the injury that commonly occurs in DAI.

The presence of axonal varicosities (Figure 4a), which is a characteristic pathology of mild TBI, in the CHIMERA injured brain, but not the sham brain (Figure 4b) was demonstrated by neurofiliament immunohistochemistry. Axonal morphology appeared to be normal in the optic tract of the sham brain with linear shape and consistent spatial dimensions across axons. In the optic tract of the injured brains, features were found that are consistent with axonal varicosities. While this suggests that changes in axonal morphology may contribute to the detected abnormalities in dPFG and FA values, it is important to note that other cellular alterations (e.g. reactive gliosis or myelin abnormalities), which were not investigated in this study are likely also present in addition to the observed axon varicosities.

4. Conclusion

dPFG MRI shows promise in detecting cellular and microstructural alterations between DAI injured and healthy brains. Efforts are underway to explore developing this method into a new quantitative imaging tool to detect TBI.

Acknowledgments

This work was supported by the Intramural Research Program of the *Eunice Kennedy Shriver* National Institute of Child Health and Human Development [grant numbers HD000266] and The Henry M. Jackson Foundation for the Advancement of Military Medicine, Inc, [HJF Award Numbers: 308049-8.01-60855 and 307513?3.01?60855].

References

1. Faul M, Xu L, Wald M, Coronado V. Traumatic Brain Injury in the United States: Emergency Department Visits, Hospitalizations and Deaths 2002–2006. Centers for Disease Control and Prevention, National Center for Injury Prevention and Control; 2010.
2. Meythaler JM, Peduzzi JD, Eleftheriou E, Novack TA. Current concepts: diffuse axonal injury-associated traumatic brain injury. Archives of Physical Medicine and Rehabilitation. 2001; 82:1461–71. [PubMed: 11588754]
3. Maxwell WL, Povlishock JT, Graham DL. A mechanistic analysis of nondisruptive axonal injury: a review. Journal of Neurotrauma. 1997; 14:419–40. [PubMed: 9257661]
4. Gaetz M. The neurophysiology of brain injury. Clinical Neurophysiology. 2004; 115:4–18. [PubMed: 14706464]
5. Namjoshi DR, Cheng WH, McInnes KA, Martens KM, Carr M, Wilkinson A, Fan J, Robert J, Hayat A, Cripton PA, Wellington CL. Merging pathology with biomechanics using CHIMERA (Closed-Head Impact Model of Engineered Rotational Acceleration): a novel, surgery-free model of traumatic brain injury. Molecular Neurodegeneration. 2014; 9:55. [PubMed: 25443413]
6. Basser PJ, Mattiello J, LeBihan D. MR diffusion tensor spectroscopy and imaging. Biophysical Journal. 1994; 66:259–67. [PubMed: 8130344]
7. Budde MD, Frank JA. Neurite beading is sufficient to decrease the apparent diffusion coefficient after ischemic stroke. Proceedings of the National Academy of Sciences. 2010; 107:14472–7.
8. Yuh EL, Cooper SR, Mukherjee P, Yue JK, Lingsma HF, Gordon WA, Valadka AB, Okonkwo DO, Schnyer DM, Vassar MJ, Maas AIR, Manley GT. TRACK-TBI INVESTIGATORS, Diffusion tensor imaging for outcome prediction in mild traumatic brain injury: a TRACK-TBI study. Journal of Neurotrauma. 2014; 31:1457–77. [PubMed: 24742275]
9. Hutchinson EB, Schwerin SC, Radomski KL, Irfanoglu MO, Juliano SL, Pierpaoli CM. Quantitative MRI and DTI Abnormalities During the Acute Period Following CCI in the Ferret. Shock. 2016; 46:167–76. [PubMed: 27294688]
10. Mitra P. Multiple wave-vector extensions of the NMR pulsed-field-gradient spin-echo diffusion measurement. Physical Review B. 1995; 51:15074–15078.
11. Komlosh ME, Özarslan E, Lizak MJ, Horkay F, Schram V, Shemesh N, Cohen Y, Basser PJ. Pore diameter mapping using double pulsed-field gradient MRI and its validation using a novel glass capillary array phantom. Journal of Magnetic Resonance. 2011; 208:128–35. [PubMed: 21084204]
12. Weber T, Ziener CH, Kampf T, Herold V, Bauer WR, Jakob PM. Measurement of apparent cell radii using a multiple wave vector diffusion experiment. Magnetic Resonance in Medicine. 2009; 61:1001–6. [PubMed: 19205023]
13. Koch MA, Finsterbusch J. Towards compartment size estimation in vivo based on double wave vector diffusion weighting. NMR in Biomedicine. 2011; 24:1422–1432. [PubMed: 21755551]
14. Komlosh ME, Özarslan E, Lizak MJ, Horkayne-Szakaly I, Freidlin RZ, Horkay F, Basser PJ. Mapping average axon diameters in porcine spinal cord white matter and rat corpus callosum using d-PFG MRI. NeuroImage. 2013; 78:210–6. [PubMed: 23583426]
15. Avram AV, Özarslan E, Sarlls JE, Basser PJ. In vivo detection of microscopic anisotropy using quadruple pulsed-field gradient (qPFG) diffusion MRI on a clinical scanner. NeuroImage. 2013; 64:229–239. [PubMed: 22939872]
16. Benjamini D, Komlosh ME, Basser PJ, Nevo U. Nonparametric pore size distribution using d-PFG: Comparison to s-PFG and migration to MRI. Journal of Magnetic Resonance. 2014; 246:36–45. [PubMed: 25064269]

17. Benjamini D, Komlosh ME, Holtzclaw LA, Nevo U, Basser PJ. White matter microstructure from nonparametric axon diameter distribution mapping. NeuroImage. 2016; 135:333–344. [PubMed: 27126002]
18. Stejskal E, Tanner J. Spin diffusion measurements: Spin echoes in the presence of a time-dependent field gradient. Journal of Chemical Physics. 1965; 42:288–292.
19. Pierpaoli C, Barnett A, Basser P, Chang L-C, Koay C, Pajevic S, Rohde G, Sarlls J, Wu M. ISMRM 18th Annual Meeting; Stockholm, Sweden: 2010. TORTOISE: an integrated software package for processing of diffusion MRI data.
20. Grebenkov DS. Laplacian eigenfunctions in NMR. I. A numerical tool. Concepts in Magnetic Resonance Part A. 2008; 32A:277–301.
21. Ozarslan E, Shemesh N, Basser PJ. A general framework to quantify the effect of restricted diffusion on the NMR signal with applications to double pulsed field gradient NMR experiments. The Journal of Chemical Physics. 2009; 130:104702. [PubMed: 19292544]
22. Ozarslan E. Compartment shape anisotropy (CSA) revealed by double pulsed field gradient MR. Journal of Magnetic Resonance. 2009; 199:56–67. [PubMed: 19398210]
23. Assaf Y, Basser PJ. Composite hindered and restricted model of diffusion (CHARMED) MR imaging of the human brain. NeuroImage. 2005; 27:48–58. [PubMed: 15979342]
24. Haber M, Hutchinson E, Irfanoglu M, Cheng W, Namjoshi D, Cripton P, Wellington C, Diaz-Arrastia R, Pierpaoli C. Society for Neurotrauma Annual conference. Lexington, KY: 2016. DTI and MAP-MRI Abnormalities in the Closed Head Injury model of engineered rotational acceleration (CHIMERA) Mouse Model of Diffuse Axonal Injury.

- A double-pulsed field gradient (dPFG) MRI sequence was proposed to detect diffuse axonal injury.
- Apparent mean axon diameters were estimated using dPFG MRI in injured and healthy fixed mouse brain tissue.
- Significantly different mean diameters were measured in injured and healthy tissues.

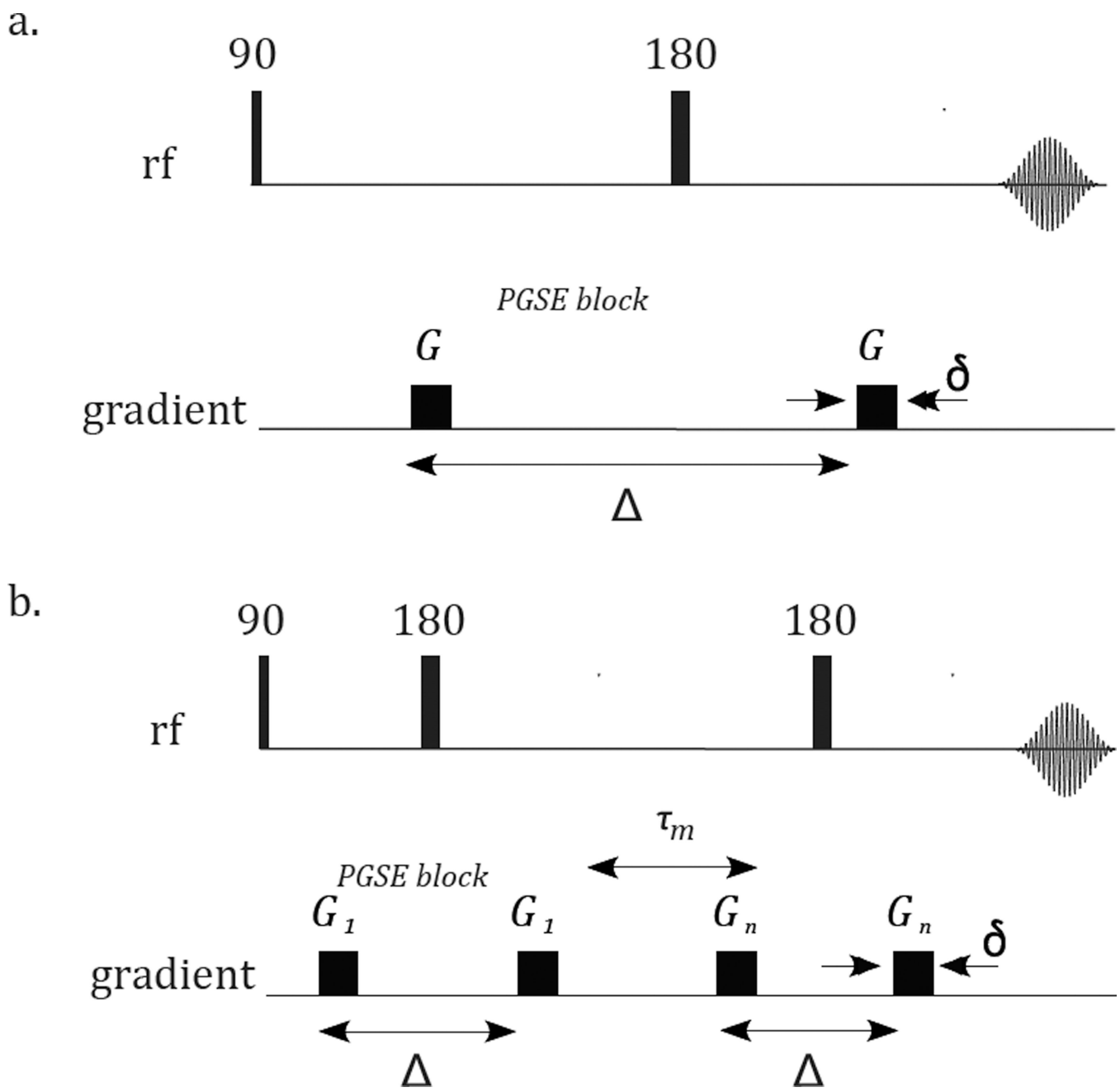

Figure 1.
Pulse sequences of a. Pulsed-field gradient [18], encoding net displacements; b. Double pulsed-field gradient, encoding diffusion correlation.

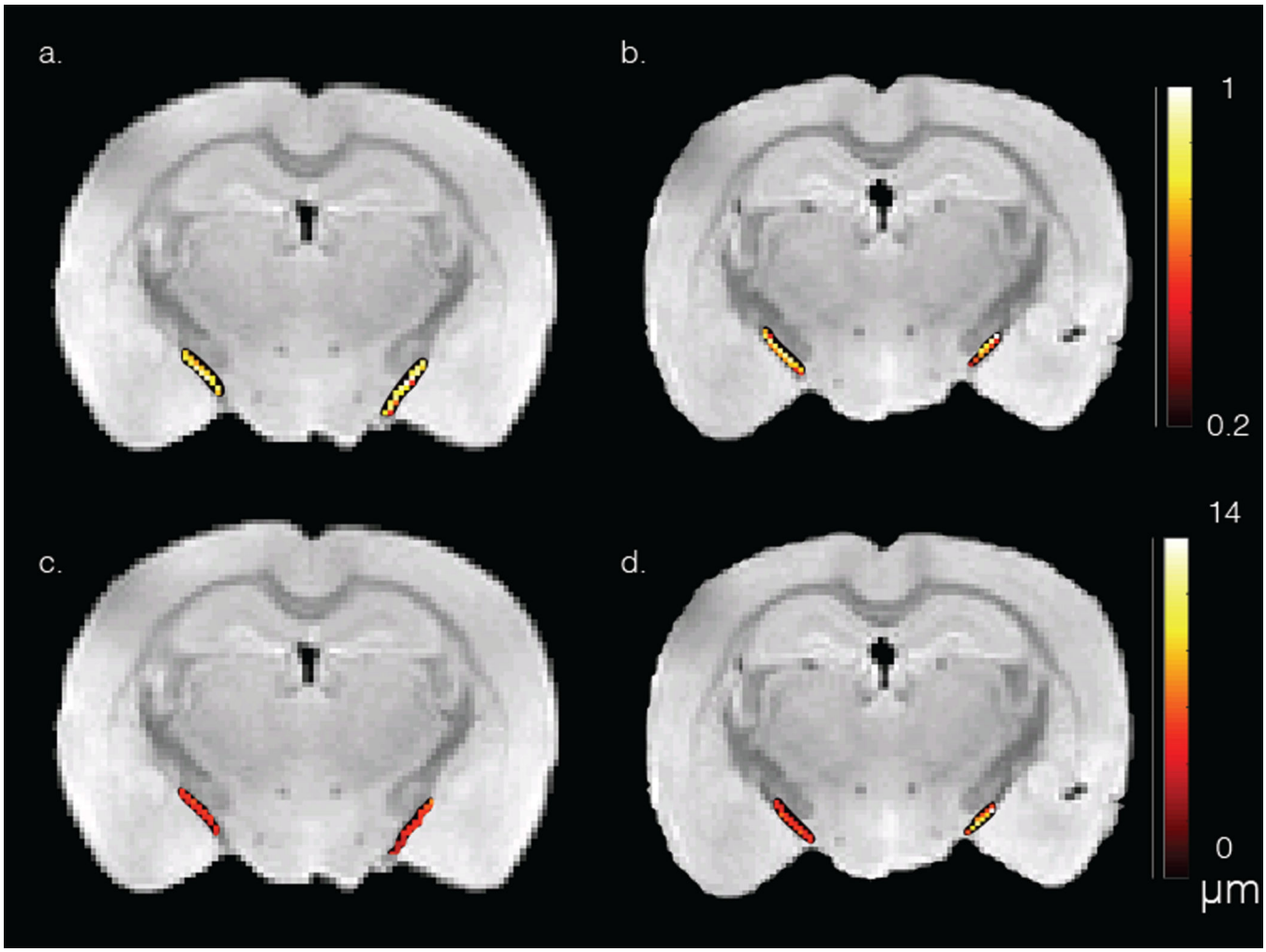

Figure 2.
DTI FA (a–b) and dPFG AMD (c–d) maps of the optic tract overlay a structural image of the sham (a, c) and CHIMERA (b, d) mouse brains.

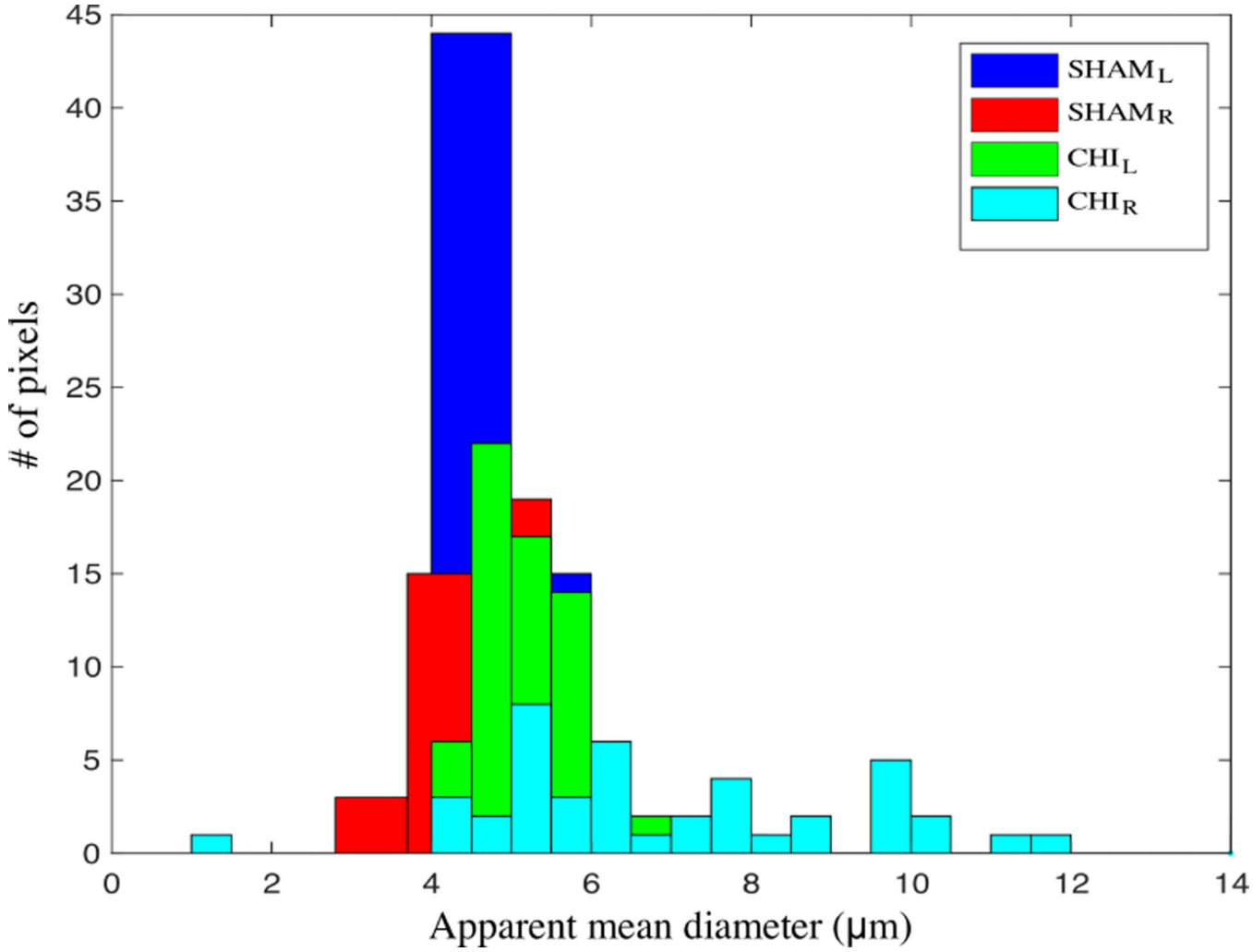

Figure 3.
Histogram of AMDs within the CHIMERA and sham optic tracts.

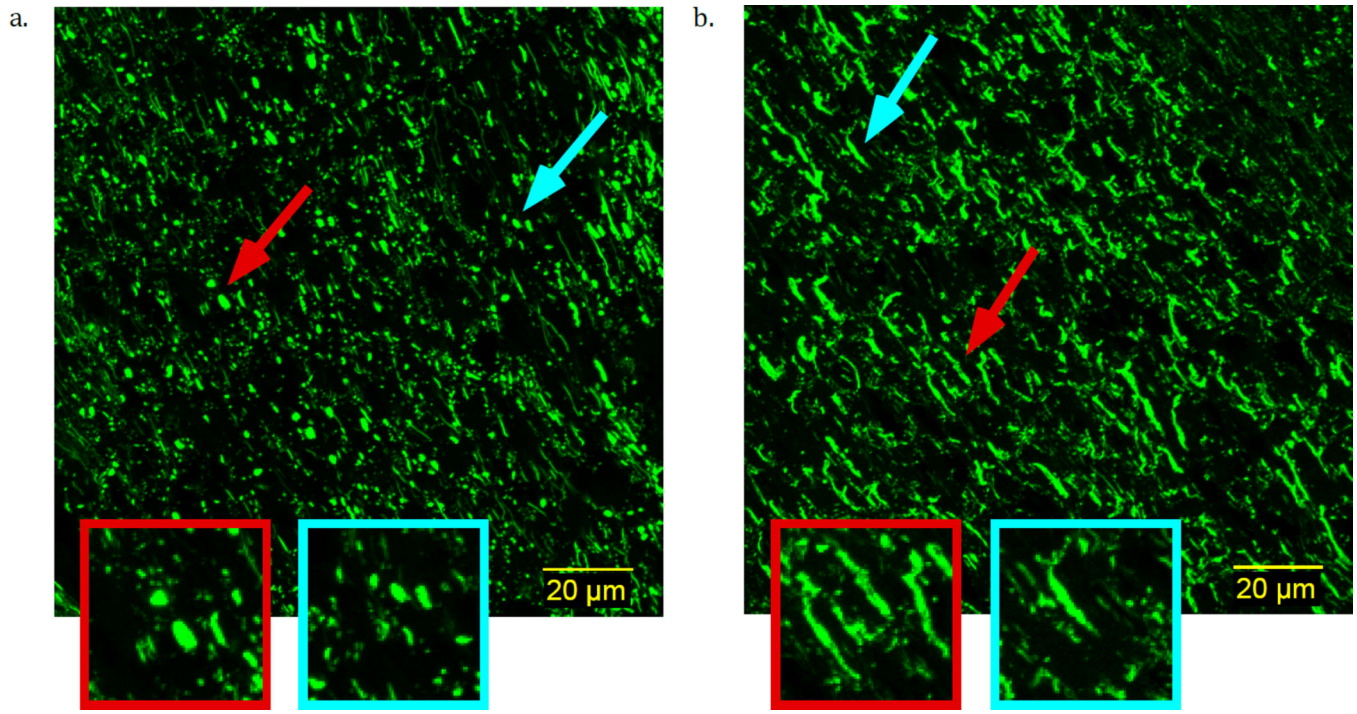

Figure 4.

Confocal microscopy images of immunohistochemistry for axonal neurofilament protein in the optic tract of a. CHIMERA and b. sham mouse brains. Examples for axonal varicosities (a) and normal shaped axon (b) are magnified.